PERGAMON

Journal of South American Earth Sciences 13 (2000) 325–336

Journal of
South American
Earth Sciences

www.elsevier.nl/locate/jsames

The Early Cretaceous Arperos basin: an oceanic domain dividing the Guerrero arc from nuclear Mexico evidenced by the geochemistry of the lavas and sediments

C. Freydier[a], H. Lapierre[a,*], J. Ruiz[b], M. Tardy[c], J. Martinez-R.[d], C. Coulon[e]

[a]*LGCA, UMR CNRS 5025, Université Joseph Fourier-Grenoble 1, BP 53, 38041-Grenoble Cedex 9, France*
[b]*Département of Geosciences, University of Arizona, Tucson, AZ 85721 USA*
[c]*LGCA, UMR CNRS 5025, Université de Savoie 73376, Le Bourget du Lac cedex, France*
[d]*Unidad de Investigacion en Ciencias de la Tierra, Univ Nac Autonoma Mexico-Juriquilla, AP 1-742, Santiago de Queretaro (Qro) 76001 Mexico*
[e]*Lab Pet Mag, URA CNRS 1277, Université d'Aix-Marseille III, BP 441, 13397 Marseille Cedex 20, France*

Abstract

During the Early Cretaceous, the Arperos basin was located between the Guerrero arc terrane and nuclear Mexico. Remnants of this basin now form an oceanic suture zone between the coeval carbonate platforms to the east and the accreted Guerrero terrane to the west. The geochemistry on the Arperos mafic hypabyssal and volcanic rocks, based on the incompatible and trace element distribution and the $\epsilon Nd_{(T=110\ Ma)}$ values, shows that this basin was floored by basalts that likely were generated by the mixing of OIB and N-MORB sources. The submarine lavas are overlain by and/or interbedded with siliceous sediments that have the highest $\epsilon Nd_{(T=110\ Ma)}$ and lowest Th levels. In contrast, the turbidites interlayered with the pelagic carbonates located at the top of the Arperos stratigraphic column show the lowest $\epsilon Nd_{(T=110\ Ma)}$ values and the highest Th contents. This evolution with time in the chemistry of the Arperos sediments is interpreted as marking the approach of the Guerrero juvenile arc to nuclear Mexico.

Keywords: Guerrero terrane; Nuclear Mexico; Arperos basin

1. Introduction

The main process in mountain building is the accretion of lithospheric fragments to the margins of cratons. In the North American Cordillera, this accretion process is often linked to the collision of islands arcs with the borderland of North America and the closure of basins floored by oceanic crust. The remnants of these oceanic basins are now represented by dismembered ophiolitic suites, or melanges, or even oceanic plateaus with their pelagic sedimentary cover. Most of these arc-accreted terranes show a continental character. However, the isotopic signatures of the igneous and sedimentary rocks of the eastern Klamath terrane (Brouxel et al., 1987; Lapierre et al., 1987), Wrangellia, Stikine, Alexander (Samson et al., 1990) and Guerrero terranes (Lapierre et al., 1992a; Centeno-Garcia et al., 1993; Tardy et al., 1994) exemplify their juvenile characteristics.

The Guerrero terrane, which forms almost 40% of all Mexico, is composed of Late Jurassic–Early Cretaceous igneous and sedimentary rocks which were developed in an intra-oceanic setting (Lapierre et al., 1992a,b; Centeno-Garcia et al., 1993; Tardy et al., 1994). Moreover, no volcanic material is present in the Albian–Cenomanian platform of eastern Mexico (Fig. 1). Thus, the Guerrero arc terrane, before its accretion to North America during the Late Cretaceous, was likely offshore and separated from nuclear Mexico by a significant oceanic domain. Questions remain on the nature of this oceanic domain and the present-day location of its remnants in western Mexico.

Where the boundary between the volcano-plutonic and/or volcano-sedimentary rocks of the Guerrero arc-terrane and the coeval platform carbonates of the Sierra Madre terrane is exposed, the Guerrero arc-rocks are thrust upon Lower Cretaceous (Davila-Alcocer and Martinez-Reyes, 1987) micritic limestones, radiolarian oozes and pillow basalts collectively known as the Arperos basin (Lapierre et al., 1992b; Tardy et al., 1994). It has been demonstrated that the Arperos basin represents an oceanic domain that divided the Guerrero intra-oceanic arc from nuclear Mexico (Freydier et al., 1996b) and currently forms an important suture between the Guerrero terrane and nuclear Mexico.

Here, we present a summary of the trace element and

* Corresponding author. Tel.: +33-4-7663-5906; fax: +33-4-7651-4058.
E-mail address: henriette.lapierre@ujf.grenoble.fr (H. Lapierre).

0895-9811/00/$ - see front matter
PII: S0895-9811(00)00027-4

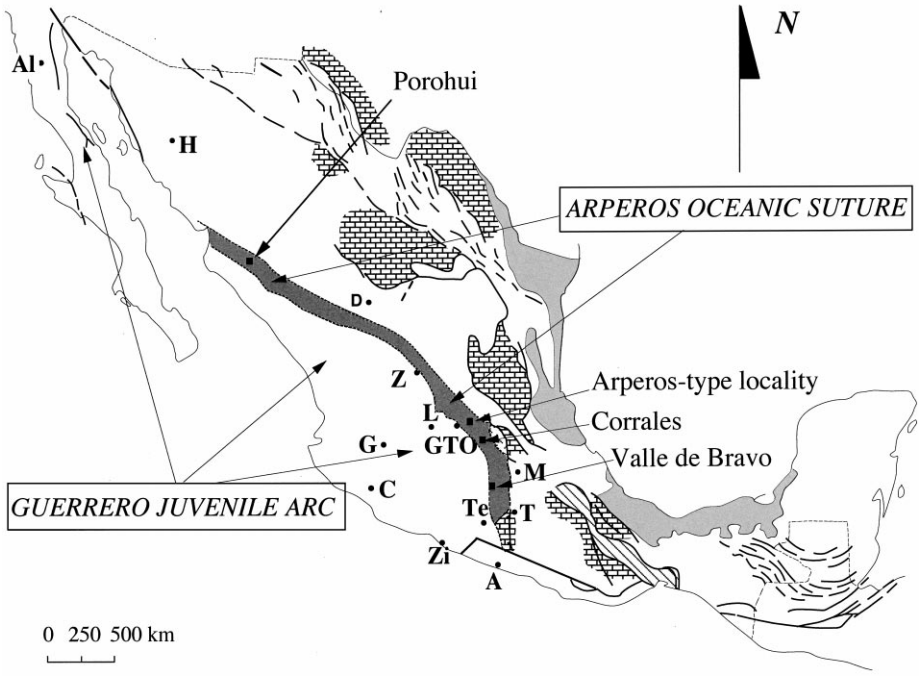

Fig. 1. Simplified map of Mexico showing the localities where the Arperos basin has been defined. This basin forms a suture between the coeval carbonate platforms to the east and the Guerrero terrane to the west. City abbreviations: A = Acapulco; Al = Alisitos; Ar = Arcelia; C = Colima; D = Durango; G = Guadalajara; GTO = Guanajuato; H = Hermosillo; M = Mexico City; T = Taxco; Te = Teloloapan; Z = Zacatecas; Zi = Zihuatanejo.

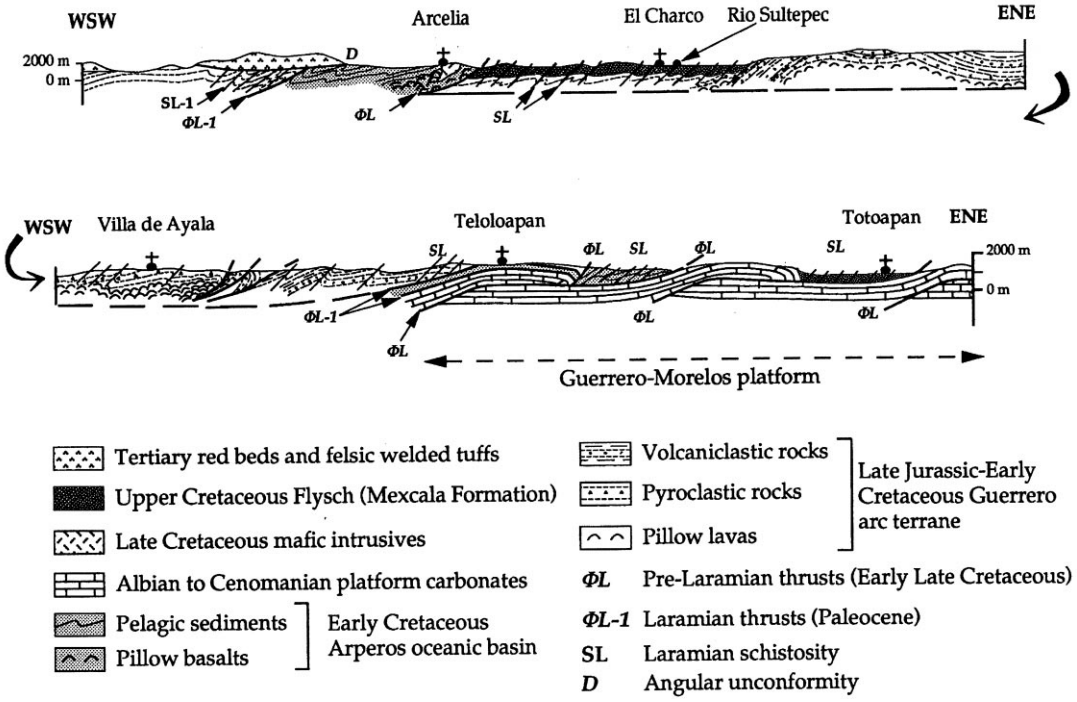

Fig. 2. Arcelia to Taxco WSW–ENE cross-section (see Fig. 1 for location) of the Guerrero terrane and the Arperos suture showing the complex tectonic relationship of the accreted arc with the Arperos basin and the carbonate platform of Guerrero-Morelos.

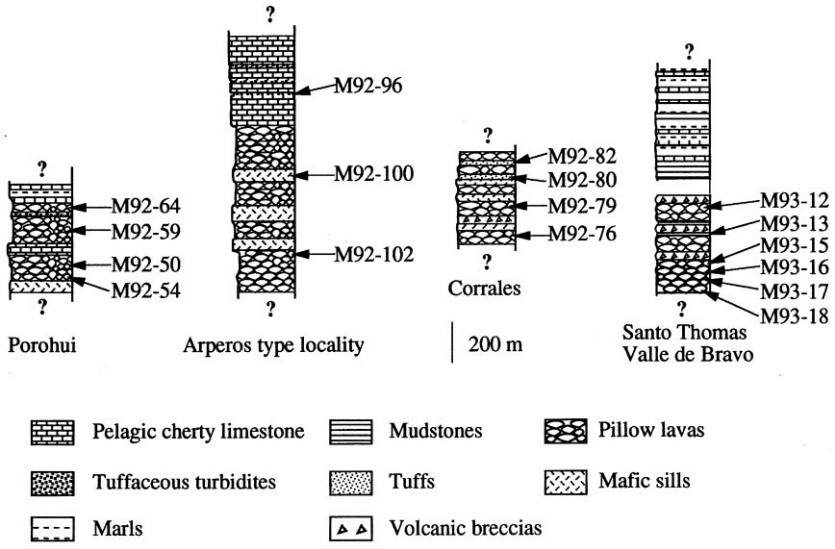

Fig. 3. Stratigraphic columns for the analyzed igneous and sedimentary rocks from the Arperos basin (see Fig. 1 for locations).

isotopic data from the igneous and sedimentary rocks of the Arperos oceanic basin that separated the Guerrero terrane from nuclear Mexico.

2. Geologic and tectonic setting of the Arperos basin

The geology of Mexico consists of two main tectono-stratigraphic terranes: (1) the Sierra Madre terrane, or the Tethyan realm after the French terminology (Tardy et al., 1986) to the east–northeast; and (2) the Guerrero terrane to the west–southwest (Campa and Coney, 1983; Campa, 1985; Coney, 1989).

The Sierra Madre terrane is composed of Upper Mesozoic and Cenozoic strata resting on a composite basement that resulted from Late Proterozoic accretions to the North American craton (Campa, 1985). During the Late Jurassic–Early Cretaceous, a transtensional regime favored the opening of the Gulf of Mexico and the intra-cratonic basins of the Sierra Madre terrane, followed by the post-Middle Jurassic through Late Cretaceous transgression assemblage. During the latter part of the Early Cretaceous, shallow water marine carbonates accumulated on the platforms while pelagic sediments filled the basins (Campa and Coney, 1983; Tardy et al., 1986). After the Turonian (~90 Ma), flysch-type sediments, which formed predominantly of arc-derived debris deposited in foreland flexural basins, were deformed and transported as nappes on the easternmost carbonate platforms during the Laramide orogeny. This flysch-type sedimentation migrated eastward and lasted until the Cenozoic.

The Guerrero terrane (Campa and Coney, 1983; Campa, 1985; Coney, 1989) is composed of Late Jurassic to Early Cretaceous subduction-related igneous and sedimentary rocks considered to be developed in an intra-oceanic setting (Lapierre et al., 1992a,b; Centeno-Garcia et al., 1993; Tardy et al., 1994). Most of the arc sequences were built on oceanic crust (Ortiz-Hernandez et al., 1991; Lapierre et al., 1992a,b; Tardy et al., 1994), locally thickened by crustal-derived sediments (Centeno-Garcia et al., 1993; Freydier et al., 1996a). However, the arc sequences exposed in Baja California (Almazan-Vazquez, 1988) and Sinaloa (Bonneau, 1972) are assumed to have a continental basement.

The boundary between the Guerrero and the Sierra Madre terranes is obscured by the Tertiary ignimbrites of the Sierra Madre Occidental. However, there are two localities — i.e. Guanajuato and Valle de Bravo (Fig. 1) — where this boundary is exposed. In these localities, the Arperos basin forms a tectonic unit caught between the Guerrero arc-rocks to the southwest and the carbonate-platforms to the northeast (Freydier et al., 1996b). This basin is represented by pillow basalts associated with pillow-breccias, tuffs and siliceous shales conformably overlain by pelagic limestones, radiolarian oozes and fine-grained turbidites (Freydier et al., 1996b) that are tectonically overlapped by the Guerrero arc-rocks (Fig. 2). The Arperos suture zone can be followed farther south near Teloloapan. There, the basin is represented by intensely deformed pelagic limestones, shales and tuffaceous green mudstones known in the literature as the Pachivia Formation (Campa and Ramirez, 1979). West of Teloloapan, near Arcelia (Fig. 1), the Arperos pillow basalts and their interlayers of siliceous shales crop out again (Fig. 2). The siliceous shales yielded Valanginian to Hauterivian (Early Cretaceous) radiolaria fauna (Salinas-Prieto, 1994). The Arperos rocks are thrust upon the Upper Cretaceous flysch-type sediments and are, in turn, tectonically overlapped by the arc tholeiites (Fig. 2). The volcanic and sedimentary assemblages of the Arperos basin are also exposed in Corrales (central Mexico; Fig. 1) and farther north near Porohui, but in these areas the relations of the Arperos rocks with the Guerrero arc rocks are not exposed. Summarizing, the Arperos basin represents an oceanic

Table 1
Geochemical characteristics of igneous rocks from the Arperos Basin (analyses performed by ICP-OES at the Laboratoire de Pétrologie Magmatique, URA CNRS 1277, Université d'Aix-Marseille III. LOI = loss on ignition)

Location	Arperos[a]	Arperos[a]	Arperos[a]	Arperos[a]	Arperos[a]	Arperos[a]	Arperos	Arperos	Valle de Bravo[a]	Valle de Bravo[a]
Sample	LP172 (Dolerite)	SF2 (Dolorite)	SF3 (Basalt)	LP167 (Basalt)	LP32 (Dolerite)	LP33B (Dolerite)	M92-100 (Dolerite)	M92-102 (Basalt)	ST2 (Basalt)	ST5 (Basalt)
SiO_2	47.4	47.3	45.3	46.0	48.0	48.3	48.3	44.0	49.1	47.5
TiO_2	2.2	2.2	2.3	2.7	2.4	2.4	2.5	2.4	1.9	2.0
Al_2O_3	16.7	16.4	15.8	17.4	16.5	16.5	16.9	15.4	15.5	15.2
Fe_2O_3	10.3	9.7	10.1	10.5	9.2	9.7	2.2	2.6	1.0	0.8
FeO							7.5	8.3	8.7	10.3
MnO	0.15	0.1	0.1	0.1	0.1	0.1	0.1	0.1	0.2	0.2
MgO	6.9	7.0	7.0	6.3	6.2	6.4	6.9	6.1	4.9	5.0
CaO	6.6	6.3	5.4	4.7	8.3	6.5	5.2	9.7	8.6	10.1
Na_2O	4.2	3.5	4.0	4.2	4.2	4.2	4.3	3.6	3.7	3.6
K_2O	1.1	2.2	1.5	1.9	1.0	1.6	1.8	1.8	0.3	0.3
P_2O_5	0.4	0.5	0.5	0.5	0.3	0.4	0.4	0.4	0.3	0.3
LOI	3.7	4.3	8.0	5.2	3.5	3.6	4.5	6.2	5.2	4.2
Total	99.8	99.8	100.0	99.8	99.7	99.8	100.6	100.7	99.3	99.4
Ni (ppm)	101	94	91	147	43	44	82	95	111	187
Cr	157	146	113	250	212	137	145	111	233	364
V	220	206	238	278	302	258	240	252	254	242
Y	38	34	37	44	37	40	40	35	41	39
Zr	192	180	153	266	215	206	239	210	246	226
Nb	19	14	5	25	21	20	26	22	15	14
Ba	97	121	146	106	138	143	116	34	406	131
Sr	323	576	333	201	304	281	398	304	229	325
Rb	13	17	17	20	11	16			5	5
La	15.6	15.1	11.6	17.4	14.4	16.1	18.9	17.6	12.9	12.5
Ce	44.1	34.7	31.3	45.4	36.8	38.3	39.7	36.1	28.2	29.4
Nd	20.5	17.8	16.9	25.9	20.6	22.7	22.8	20.5	18.8	18.2
Sm	5.6	5.1	5.2	7.7	6.0	6.8	5.5	5.2	5.2	5.0
Eu	1.8	1.6	1.6	2.3	2.0	2.1	2.0	1.9	1.5	1.5
Gd	6.6	5.4	5.5	8.0	6.1	6.8	7.4	6.7	6.5	6.4
Dy	6.3	5.3	5.7	7.8	6.5	7.0	6.7	6.3	6.7	6.7
Ho									1.3	1.2
Yb	3.0	2.6	2.9	4.0	3.4	3.6	3.5	2.8	3.8	3.6
Lu	0.6	0.3	0.6	0.7	0.3	0.6	0.5	0.4	0.6	0.5
Eu/Eu^*	0.9	1.0	0.9	0.9	1.0	1.0	1.0	1.0	0.8	0.8
$(La/Yb)_N$	3.5	3.9	2.7	3.0	2.9	3.0	3.7	4.3	2.3	2.3
Zr/Nb	10.1	12.9	30.6	10.6	10.2	10.3	9.2	9.5	16.4	16.1
ZrY	5.1	5.3	4.1	6.0	5.8	5.2	6.0	6.0	6.0	5.8
Ti/Zr	68.8	74.7	91.8	62.0	68.4	70.2	62.3	67.4	47.1	52.3
Nb/Sm	3.39	2.75	0.96	3.25	3.5	2.94	4.73	4.23	2.88	2.8
Nb/Yb	6.33	5.38	1.72	6.25	6.18	5.56	7.43	7.86	3.95	3.89
La/Nb	0.8	1.1	2.3	0.7	0.7	0.8	0.7	0.8	0.9	0.9

Table 1 (*continued*)

Location	Valle de Bravo	Valle de Bravo	Valle de Bravo	Valle de Bravo	Porohui	Porohui	Porohui	Porohui	Corrales	Corrales
Sample	M93-12 (Basalt)	M93-15 (Dolorite)	M93-17 (Basalt)	M93-18 (Basalt)	M92-54 (Dolorite)	M92-59 (Dolorite)	M92-64 (Basalt)	M92-65 (Basalt)	M92-76 (Benmoreite)	M92-79 (Benmoreite)
SiO_2	51.7	45.8	44.5	47.1	48.4	48.5	44.1	41.3	61.7	59.1
TiO_2	2.1	1.9	0.9	1.0	2.1	1.3	2.1	1.5	1.3	1.5
Al_2O_3	16.8	15.0	15.1	17.5	15.7	15.4	16.5	14.6	12.2	14.4
Fe_2O_3	1.3	1.5	0.9	1.0	1.7	8.4	1.5	3.0	2.3	2.2
FeO	4.9	6.82	7.0	6.7	8.1		8.4	7.1	5.0	6.4
MnO	0.1	0.1	0.1	0.1	0.2	0.1	0.1	0.2	0.1	0.1
MgO	4.3	5.0	6.4	6.7	7.7	8.2	8.0	7.9	4.7	3.5
CaO	4.7	12.3	12.6	8.0	7.7	10.5	6.3	10.8	4.0	4.3
Na_2O	6.5	4.1	4.1	4.2	3.4	3.3	3.7	3.3	3.9	3.9
K_2O	0.7	0.2	0.2	0.9	0.8	0.4	1.2	0.1	0.03	-
P_2O_5	0.5	0.3	0.1	0.1	0.2	0.1	0.4	0.2	0.2	0.5
LOI	5.4	6.6	7.4	5.2	4.0	2.8	7.2	9.5	4.1	3.1
Total	98.9	99.7	99.3	98.6	99.9	99.0	99.3	99.7	99.4	99.0
Ni (ppm)	106	177	146	141	86	42	50	105	25	0
Cr	202	269	287	318	198	205	217	287	25	4
V	222	196	204	173	273	289	278	208	250	139
Y	46	39	23	25	36	38	33	28	31	66
Zr	189	170	63	70	144	174	145	93	94	410
Nb	12	12	2	3	8	11	9	6	5	10
Ba	358	72	18	111	109	498	467	55	23	25
Sr	264	249	319	240	324	510	416	261	72	112
Rb	3	5	8	12	8	22	16	6	6	2
La	11.2	11.3	10.7	3.1	9.1	14.7	11.4	6.5	5.3	10.1
Ce	29.8	28.4	27.1	9.1	21.5	36.3	28.5	16.5	15.0	27.5
Nd	20.9	18.6	18.9	8.5	16.3	25.0	18.6	12.1	11.0	24.1
Sm	5.5	4.6	4.5	2.4	4.3	5.1	5.0	3.7	3.8	7.9
Eu	1.8	1.7	1.7	1.0	1.5	1.9	1.6	1.2	1.2	2.1
Gd	9.3	7.9	4.9	4.8	6.0	6.9	5.8	4.6	4.9	10.9
Dy	7.6	6.3	6.1	4.0	5.6	6.8	5.6	4.6	5.1	11.4
Ho					1.0	1.3				2.1
Yb	3.8	3.2	3.2	2.1	2.6	2.9	3.0	2.5	3.2	6.6
Lu	0.7	0.6	0.5	0.3	0.3	0.2	0.4	0.3	0.5	0.9
Eu/Eu^*	0.8	0.9	0.9	0.9	0.9	1.0	0.9	0.9	0.8	0.7
$(La/Yb)_N$	2.0	2.4	2.3	1.0	2.3	3.4	2.5	1.7	1.1	1.0
Zr/Nb	15.8	14.2	31.5	23.3	18.0	15.8	16.1	15.5	18.8	41.0
ZrY	4.1	4.4	2.7	2.8	4.0	4.6	4.4	3.3	3.0	6.2
Ti/Zr	66.00	67.8	85.7	86.6	85.4	44.8	86.9	99.4	83.00	22.2
Nb/Sm	2.18	2.61	0.44	1.25	1.86	2.16	1.80	1.62	1.32	1.27
Nb/Yb	3.16	3.75	0.63	1.43	3.08	3.79	3.00	2.4	1.56	1.52
La/Nb	0.9	0.9	5.4	1.0	1.1	1.3	1.3	1.1	1.1	1.0

[a] From Ortiz-Hernandez (1992); basalts sampled by Enrique Ortiz

Table 2
Whole-rock Rb/Sr and Sm/Nd isotope data for igneous rocks from the Arperos basin (analyses performed at the Laboratoire de Géochimie, University of Montpellier II, after techniques described by Birck and Allègre (1978), Nakamura (1974) and Richard et al. (1976). ϵNd caluclated using $^{143}Nd/^{144}Nd = 0.512638$ as the present-day. CHUR value, $^{147}Sm/^{144}Nd$ CHUR = 0.1966.)

Location	Sample	Sr	Rb	$^{87}Rb/^{86}Sr$	$^{87}Sr/^{86}Sr$	ϵSr (110 Ma)	Nd	Sm	$^{147}Sm/^{144}Nd$	$^{143}Nd/^{144}Nd$	ϵNd (110 Ma)
Arperos	M92-100	398	5	0.036	0.704486 ± 34	+ 0.8	22.8	5.5	0.145316	0.512921 ± 16	+ 6.2
Arperos	M92-102	304	5	0.048	0.704746 ± 21	+ 4.3	20.5	5.18	0.1528	0.512872 ± 9	+5.2
Valle de Bravo	M93-12	264	3	0.033	0.704842 ± 65	+ 6.0	20.9	5.54	0.160266	0.513017 ± 42	+ 7.8
Valle de Bravo	M93-15	249	5	0.058	0.704524 ± 115	+0.9	18.6	4.57	0.1486	0.513232 ± 32	+ 12.3
Valle de Bravo	M93-17	319	8	0.072	0.704515 ± 91	+ 0.4	18.9	4.5	0.143956	0.513027 ± 13	+ 8.2
Valle de Bravo	M93-18	240	12	0.144	0.704579 ± 20	-0.3	8.5	2.4	0.17103	0.513179 ± 6	+ 10.9
Porohui	M92-50	349	4	0.033	0.704389 ± 29	-0.48	14.7	4.38	0.18015	0.512997 ± 36	+ 7.2
Porohui	M92-54	324	8	0.071	0.704626 ± 125	2	16.3	4.25	0.1576	0.512911 ± 28	+ 5.9
Porohui	M92-59	510	22	0.125	0.704810 ± 13	3.5	25	5.09	0.1231	0.512949 ± 4	+7.1
Porohui	M92-64	416	16	0.111	0.704066 ± 22	+ 1.6	18.6	5.0	0.161877	0.512912 ± 48	+ 5.8
Corrales	M92-76	72	18	0.723	0.704071 ± 24	-20.3	11	3.8	0.20722	0.513068 ± 7	+ 8.2
Corrales	M92-76	112	2	0.0516	0.703903 ± 83	-7.8	24.7	7.9	0.193137	0.513082 ± 13	+ 8.7

domain that divided the Guerrero intra-oceanic arc from nuclear Mexico. This basin was floored by basalts and was filled first by pelagic carbonaceous and siliceous sediments. With time, the sedimentation became more and more carbonate-rich with locally fine-grained turbidites (Fig. 3).

The deformations observed in the Arperos sediments and the Guerrero arc-rocks along the main thrusts verge ENE, with asymmetric folds associated with axial plane cleavage S1 and shear zones dipping WSW. Locally, a second deformation is observed which is characterized by a space cleavage S2 striking N120°E and dipping 80° to the east. This S2

Table 3
Trace element and whole-rock Sm/Nd isotope data for sediments of the Arperos basin (Values in ppm, analyses performed by inductively coupled plasma mass spectrometry, following the procedure of Hollocher and Ruiz (1995). Exact sample locations may be obtained from the authors. Isotope analyses performed after the techniques described in Patchett and Ruiz (1987). Errors are less than ±0.5% for $^{147}Sm/^{144}Nd$. Initial ϵNd calculated with ages of 110 Ma.)

Type Locality	Tuffaceous black shales		Tuffites		Fine-grained sandstone
	Valle de Bravo		Corrales		Arperos type-locality
Sample	M93-13	M93-16	M92-80	M92-82	M92-96
La	10.5	12.54	4.22	5.04	12.64
Ce	38.69	24.71	13.95	15.77	34.01
Pr	4.31	3.27	2.19	2.55	3.96
Nd	20.46	13.99	10.89	16.01	15.52
Sm	6.01	4.32	3.85	4.31	3.71
Eu	1.92	1.53	1.4	1.39	0.89
Gd	7.1	6.06	4.28	5.53	3.32
Tb	1.22	1.13	0.76	0.96	0.54
Dy	8.35	6.96	5.24	6.31	3.19
Ho	1.66	1.56	0.97	1.2	0.62
Er	5.07	4.1	3.1	3.26	1.78
Tm	0.69	0.6	0.41	0.46	0.29
Yb	4.68	3.24	2.92	2.79	1.77
Lu	0.64	0.56	0.44	0.4	0.24
$(La/Yb)_N$	1.5	2.61	0.97	1.21	4.81
Ce/Ce*	1.38	0.92	1.07	1.05	1.15
Eu/Eu*	0.89	1.22	1.05	0.87	0.7
Th	0.6	0.59	0.23	1.92	4.06
Sm (ppm)[a]	5.85	3.85	3.63	3.83	3.79
Nd (ppm)[a]	21.53	12.76	11	16.87	17.29
$^{147}Sm/^{144}Nd$[a]	0.1644	0.1823	0.1995	0.1372	0.1325
$^{143}Nd/^{144}Nd$[b]	0.513012 ± 5	0.513046 ± 7	0.513130 ± 6	0.512826 ± 6	0.512662 ± 7
ϵNd (present day)[c]	+ 7.29	+ 8.01	+ 9.4	+ 3.7	+ 0.5
ϵNd (T = 110 Ma)[c]	+ 7.75	+ 8.3	+ 9.4	+ 4.5	+ 1.4

[a] 2σ errors for $^{147}Sm/^{144}Nd$ are reproducible to <0.5%.
[b] Ratios normalized to $^{146}Nd/^{144}Nd = 0.7219$ (2σ errors reflect in-run precision).
[c] ϵNd calculated using $^{143}Nd/^{144}Nd = 0.512638$ and $^{147}Sm/^{144}Nd = 0.1966$ as present-day CHUR values.

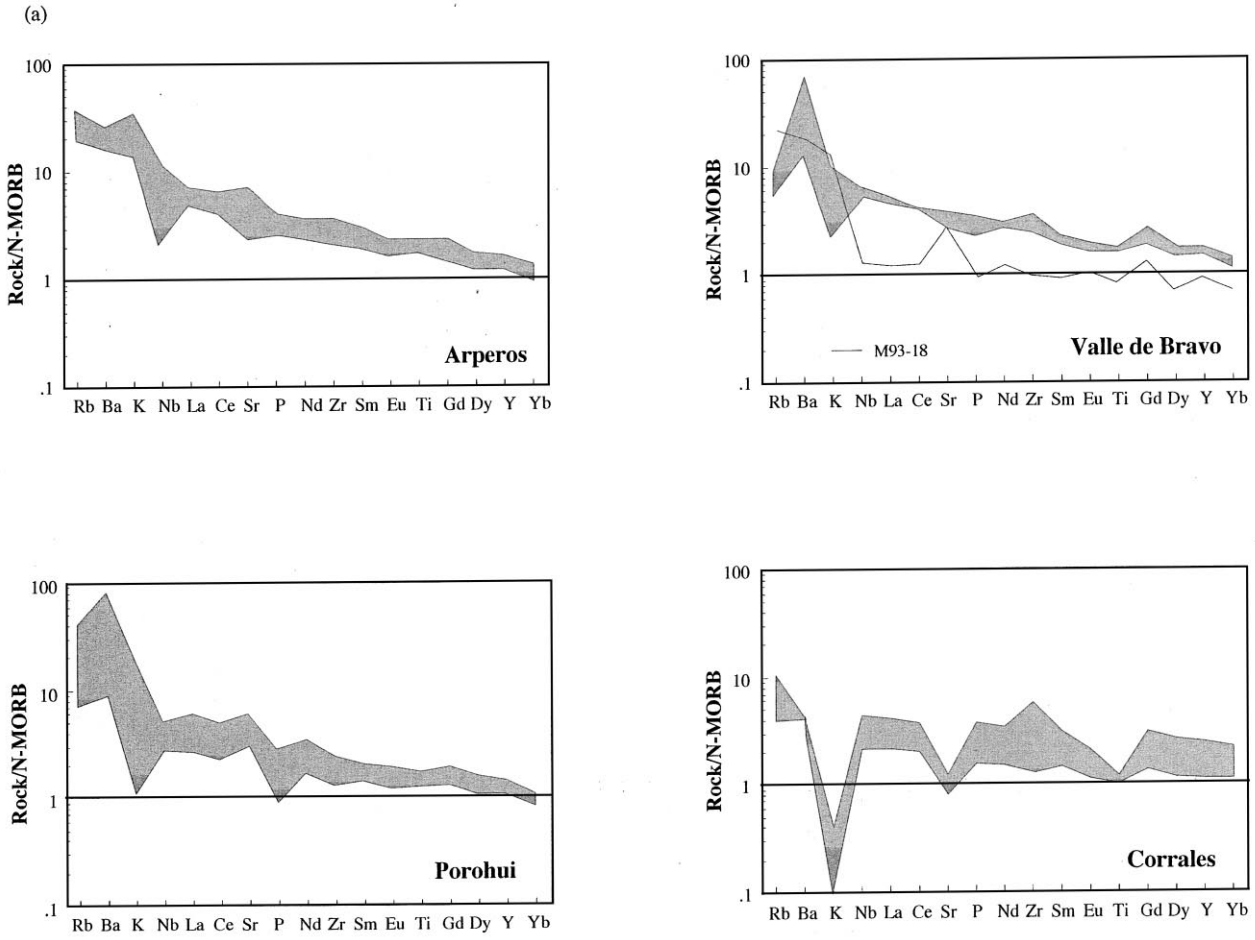

Fig. 4. (a) N-MORB normalized (Sun and McDonough, 1989) spidergrams for igneous rocks from the Arperos basin. (b) Chondrite-normalized (Evensen et al., 1978) REE patterns for igneous rocks from the Arperos basin.

is parallel to the axial planes of the ENE-verging asymmetric folds (Fig. 2).

3. Geochemistry of the igneous and sedimentary rocks from the Arperos basin

The igneous rocks from the Arperos basin are olivine-phyric and olivine-free basalts and dolerites with Ti-rich augites, characteristic of anorogenic and alkali basalts. The lavas from Corrales show trachytoid textures and are more fractionated melts, compared to the basalts and dolerites from the other exposures of the Arperos basin (Freydier et al., 1996b). All these rocks have undergone low-grade hydrothermal alteration. All the minerals are altered, with the exception of the clinopyroxenes. Olivine is replaced by serpentine, chlorite or calcite. Plagioclase is transformed to albite or adularia. The mesostasis is replaced by chlorite + prehnite + pumpellyite. The vesicles are filled with calcite or epidote or chlorite + prehnite + pumpellyite.

In order to determine the magmatic affinity of the basalts and dolerites, and the source of the sediments from the Arperos basin, major, trace and rare earth elements (REE), as well as Nd isotopes, were determined for the lavas and sediments representative of localities where the Arperos basin was defined (Tables 1–3). The locations of the analyzed samples for geochemistry are shown in Figs. 1 and 3. For more details refer to Freydier et al. (1996b).

Most of the lavas from the Arperos basin are altered, as shown by the presence of secondary minerals such as albite, smectite, prehnite, pumpellyite, calcite, epidote, chlorite, actinolite, oxide and sometimes chalcedony. Geochemically, this alteration is mainly expressed by high loss on ignition (LOI) values (Table 1). Studies on major and trace element mobility during alteration processes conclude that, generally, the more mobile elements are the alkalis (K, Na, Rb), alkaline earths (Sr, Ba, Ca, Mg), and most of the remaining major elements such as Si, Fe and Mn. These possibly mobile elements are presented below for information, but they are not discussed in detail. In some rare cases, a slight REE mobility can also occur. In contrast, Ti, Al, Nb, Y, Th, Ta, Zr, Hf, and most of the REE are considered as the less-mobile elements and are preferentially used.

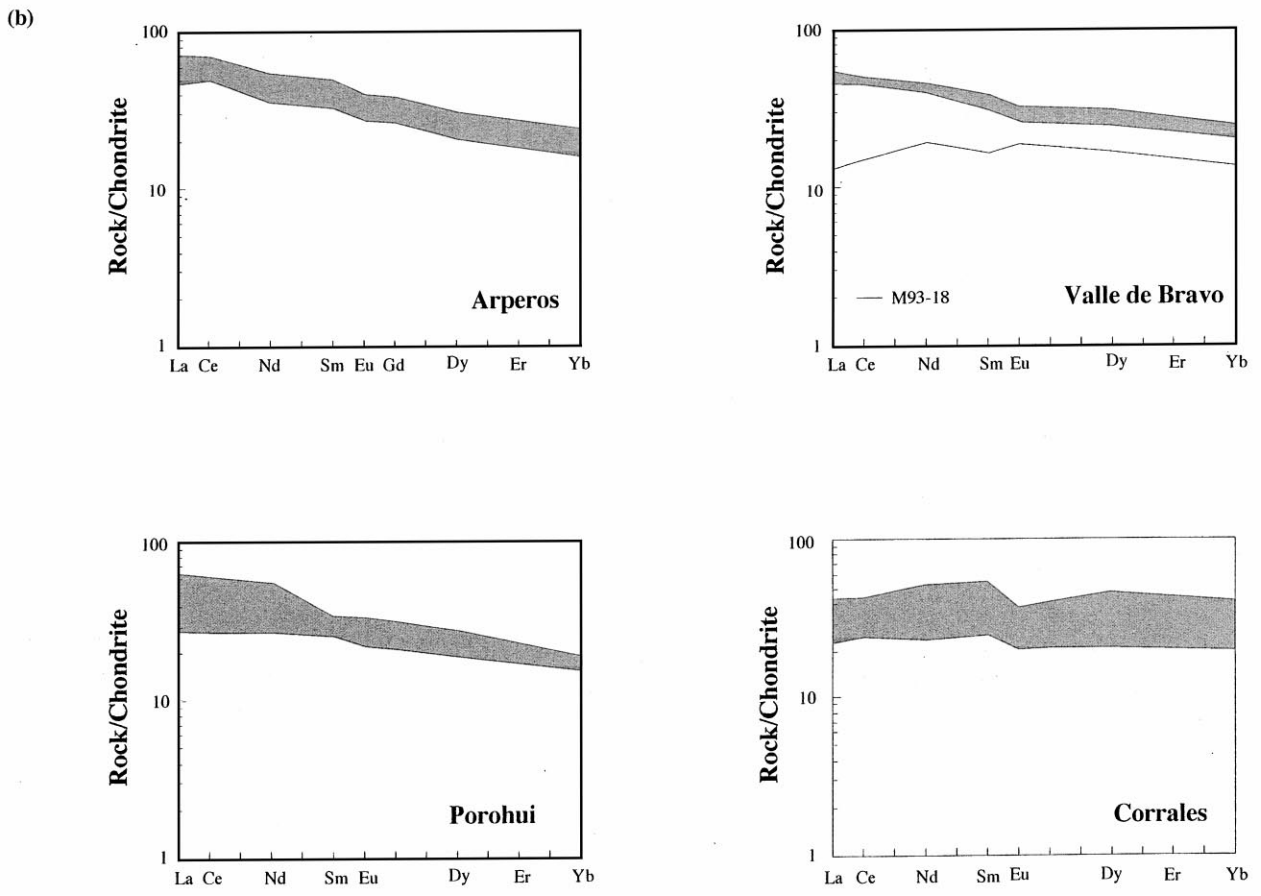

Fig. 4. (*continued*)

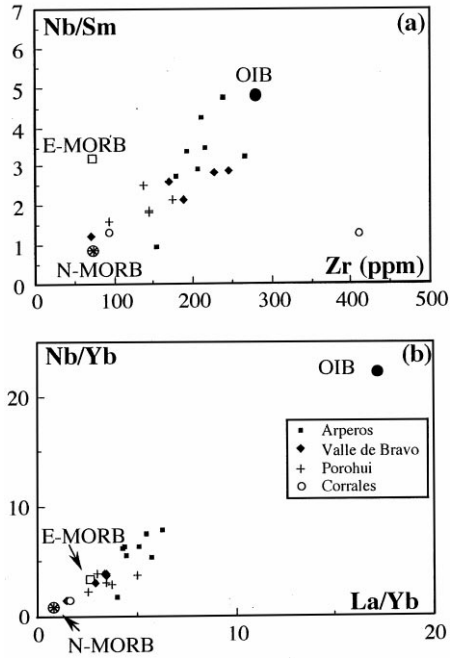

Fig. 5. Trace element ratio plots for igneous rocks from the Arperos basin. The OIB, N-MORB and E-MORB fields are from Sun and McDonough (1989): (a) Nb/Sm versus Zr; and (b) Nb/Yb versus La/Yb.

3.1. Trace element and isotopic chemistry of the basalts and dolerites

Two groups can be distinguished within the basalts and dolerites from the Arperos basin on the basis of their TiO_2 and P_2O_5 contents and their trace element distribution (for more details, refer to Freydier et al., 1996b). Group 1 includes almost all the rocks — i.e. Arperos-type locality, Porohui and Valle de Bravo, with the exception of an aphyric basalt from Valle de Bravo; Group 1 is geochemically similar to oceanic island alkali (OIA) basalts. Group 2 is composed of the lavas from Corrales and the aphyric basalt from Valle de Bravo and shows features of oceanic island tholeiites (OIT) or normal mid-oceanic ridge basalts (N-MORB).

Group 1 is enriched in large ion lithophile (LIL) and high field strength elements (HFSE) (Fig. 4a), but the LIL enrichment is greater than the HFSE. The REE patterns are light REE-enriched $[(La/Yb)_N = 1.724.28]$ (Fig. 4b), but this enrichment is lower than in ocean island basalts (OIB).

Group 2 displays flat REE patterns (Fig. 4b) and its trace element distribution is similar to N-MORB (Fig. 4a).

In the Nb/Sm versus Zr and Nb/Y versus La/Yb plots (Fig. 5), the igneous rocks from the Arperos basin fall between the N-MORB and OIB poles, with the following

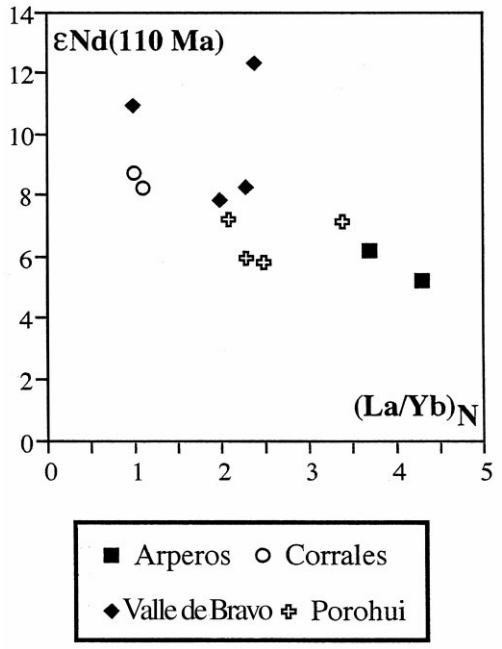

Fig. 6. $(La/Yb)_N$ versus initial $\epsilon Nd_{(T=110\ Ma)}$ plot of igneous rocks from the Arperos basin.

distribution:

- basalts and dolerites from the Arperos-type locality (Fig. 1) are the closest to the OIB pole;
- Group 2 and a basalt from Porohui (M92-65; Fig. 1) fall near the N-MORB pole; all these rocks are characterized by low Nb/Sm ratios (Fig. 5a);
- the remaining basalts and dolerites from Porohui and Valle de Bravo (Fig. 1) show compositions intermediate between the OIB and N-MORB poles and cluster near the E-MORB plot (Fig. 5). However, their Nb/Sm ratios are lower than those of E-MORB.

Thus, the lavas and hypabyssal rocks from the Arperos basin show transitional features between N-MORB and OIB and are likely derived from the mixing between OIB and N-MORB sources.

The igneous rocks from the Arperos basin show positive $\epsilon Nd_{(T=110\ Ma)}$ values that range from +5.8 to 11 (Table 2). Group 2 shows the higher values (+11 to +8.5) whereas the $\epsilon Nd_{(T=110\ Ma)}$ values of Group 1 are far more homogeneous, with a mean around +6. In the $(La/Yb)_N$ versus $\epsilon Nd_{(T=110\ Ma)}$ plot (Fig. 6), Group 1 rocks characterized by the highest LREE enrichments show the lowest $\epsilon Nd_{(T=110\ Ma)}$, +6, that falls in the range of OIB values. In contrast, Group 2 rocks are the most LREE depleted and the $\epsilon Nd_{(T=110\ Ma)}$ values approach those of N-MORB. Moreover, like the contemporaneous mafic rocks of the Caribbean–Colombian oceanic plateau, the igneous rocks from the Arperos basin exhibit Pb isotopic compositions of lavas derived from ridge-centered or near-ridge hotspots (Freydier et al., 1998; Lapierre et al., 2000).

3.2. Trace element and isotopic chemistry of the sediments

The samples of sedimentary rocks analyzed for geochemistry are representative of the lower, middle and upper parts of the Arperos stratigraphic column. Their relative location is based on sedimentary criteria.

Samples M93-13 and M93-16 were collected from the Valle de Bravo section (Fig. 1). They are tuffaceous black shales interbedded with pillow basalts or occurring as the matrix of the pillows (Figs. 1 and 3). These very fine-grained tuffaceous rocks are formed of broken feldspars and pseudomorphs of mafic minerals caught in a shaley matrix. They represent the lowermost levels of the Arperos stratigraphic column.

Samples M92-80 and M92-82 are tuffites interbedded with the subtrachytic differentiated pillows of Corrales (Figs. 1 and 3). M92-80 is a lithified ash (fragments <2 mm) formed exclusively of feldspar fragments. M92-82 is a lithic-crystal tuff with broken or whole plagioclase, Fe–Ti oxides and mafic mineral crystals replaced by epidote and calcite enclosed in an argillaceous matrix. The lithic fragments are composed of recrystallized quenched glass in which are enclosed a few feldspar microlites. Because of the presence of siliceous sediments conformably resting above the pillows and the fractionated character of lavas, we assume that these tuffites are located near the middle part of the Arperos stratigraphic column.

Finally, sample M92-96 is a fine-grained sandstone interbedded with micritic limestones and radiolarian oozes that are present at the top of the Arperos stratigraphic column (Figs. 1 and 3). This sandstone consists of rounded quartz, plagioclase crystals and altered mafic minerals in an argillaceous matrix and deposited by turbiditic currents.

The tuffaceous shales from Valle de Bravo exhibit moderatly enriched LREE patterns [$(La/Yb)_N = 1.5–2.6$]; Table 3 and Fig. 7b] whereas the tuffites from Corrales show flat [$(La/Yb)_N = 1.21$] to slightly LREE-depleted patterns [$(La/Yb)_N = 0.92$; Table 3 and Fig. 7b]. The turbidite from the Arperos type locality differs from the previous rocks by a significant LREE enrichment [$(La/Yb)_N = 4.06$; Fig. 7]. All these sedimentary rocks exhibit positive Ce anomalies with the exception of sample M93-16. All the rocks have low Th contents ($Th < 2$ ppm; Table 3), with the exception of the fine-grained turbidite, and positive $\epsilon Nd_{(T=110\ Ma)}$ values ranging between +1 and +9. Fig. 8 illustrates the good correlation that exists between $\epsilon Nd_{(T=110\ Ma)}$ values and Th in the Arperos sediments. This correlation suggests that the source of the sediments to the basin changed with time. The earliest sediments in the basin were shed from the arc or ocean floor. The latest stages of sedimentation record other, more geochemically evolved, sources that could include nuclear Mexico.

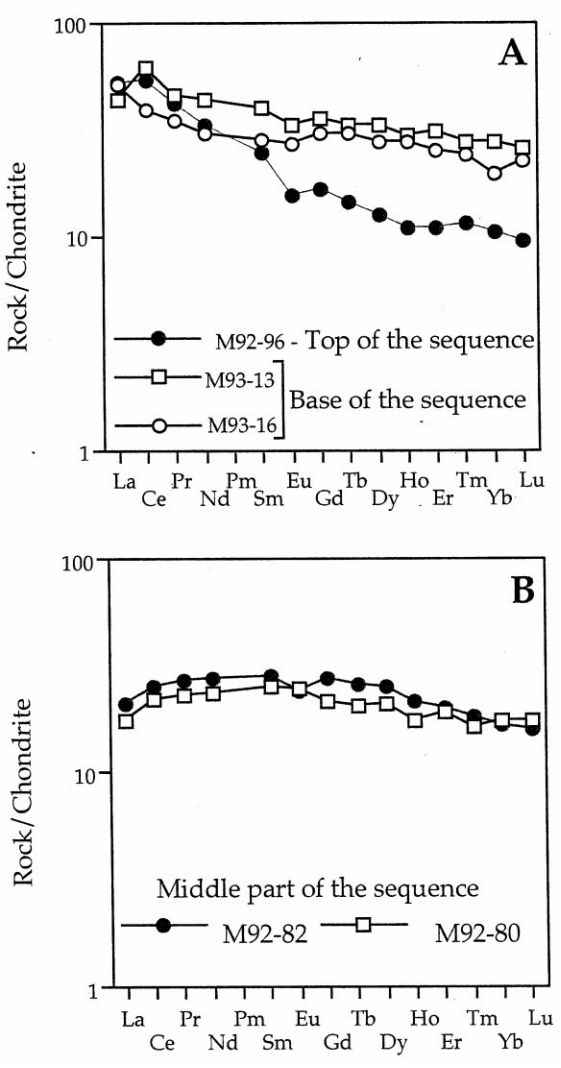

Fig. 7. Chondrite-normalized (Evensen et al., 1978) REE patterns for sedimentary rocks from the Arperos basin: (A) tuffaceous black shales and fine-grained turbidite; and (B) siliceous and tuffaceous argillites.

4. Discussion

The submarine lavas and hypabyssal rocks present at the base of the Arperos stratigraphic column contain Ti-rich clinopyroxenes characteristic of anorogenic and alkali basalts. Their geochemistry is similar to OIT, but they show transitional features between OIB and N-MORB. The basalts and dolerites from the Arperos-type locality are close to OIB because their Zr/Nb ratios are less than 10 and their $\epsilon Nd_{(T=110\ Ma)}$ values are around +6. In contrast, the aphyric basalts from Valle de Bravo and the trachytoid lavas from Corrales, with their flat to depleted LREE patterns and their high Zr/Nb (>30) and $\epsilon Nd_{(T=110\ Ma)}$ (+8 to +11) values, are close to N-MORB. The igneous rocks from Porohui exhibit transitional features between these two extremes.

The basalts and dolerites of the Arperos basin are geochemically similar to the lavas emitted in the Galapagos Islands (Vicenzi et al., 1990; Freydier et al., 1996b).

The chemistry of Arperos sediments is largely dependent on the location of these sediments in the stratigraphic column and reflects the source from which they were derived. The tuffaceous black shales located at the base of the sequence are geochemically similar to the OIT pillow basalts with which they are associated: mildly enriched LREE patterns and similar $\epsilon Nd_{(T=110\ Ma)}$ values, $\sim +7$ (Tables 2 and 3). The lithified ash (M92-80) interbedded with the trachytoid pillow basalts (M92-79) at the middle part of the stratigraphic column is similar to the surrounding lavas: LREE depleted patterns and high $\epsilon Nd_{(T=110\ Ma)}$ values (+8.7 to +9; Tables 2 and 3). The lithic-crystal tuff differs from the trachytoid basalts and the lithified ash by a lower $\epsilon Nd_{(T=110\ Ma)}$ value (+4.5) and is likely derived from the nearby juvenile arc or from the underlying oceanic basalts. Finally, the inferred uppermost sandstone is derived from a more evolved source based on its LREE enriched pattern and lower $\epsilon Nd_{(T=110\ Ma)}$ value (+1.3; Table 3). Moreover, the increase in Th contents of the Arperos sediments correlates with the decrease of their $\epsilon Nd_{(T=110\ Ma)}$ and may be explained by their evolution with time.

The Early Cretaceous Arperos basin was likely floored by oceanic crust thickened by mantle plume-type magmas whose remnants are the tholeiitic basalts and diabases exposed at the base of the Arperos stratigraphic column (Freydier et al., 1996b). The chemical evolution of the sediments with time suggests that the Guerrero arc terrane was approaching nuclear Mexico and that the Arperos basin was filled by sediments likely derived from the Sierra Madre terrane. This chemical evolution may also be related to a rise in platform topography with respect to the arc. This interpretation, however, is not possible because, during its development, the arc must have gained mass and elevation with time. Indeed, this is the case because, at the end of arc evolution during Albian–Cenomanian time, the arc-volcanic rocks became interbedded with reef limestones similar to those deposited at the same time on the platforms of the Sierra Madre terrane.

The Nd isotope data of the Guerrero arc rocks (Lapierre et al., 1992a,b; Centeno-Garcia et al., 1993) and the Arteaga Complex, which is considered the basement of the Guerrero terrane (Centeno-Garcia et al., 1993), show that this arc terrane was built on oceanic crust locally thickened by sediments (Freydier et al., 1996b) derived from the erosion of a Proterozoic crust (Centeno-Garcia et al., 1993). The geochemistry of the igneous and sedimentary rocks from the Arperos basin presented here confirms the intra-oceanic environment of the Guerrero arc.

5. Conclusions

The petrology and geochemistry of the igneous and sedimentary rocks from the Arperos basin clearly demonstrate

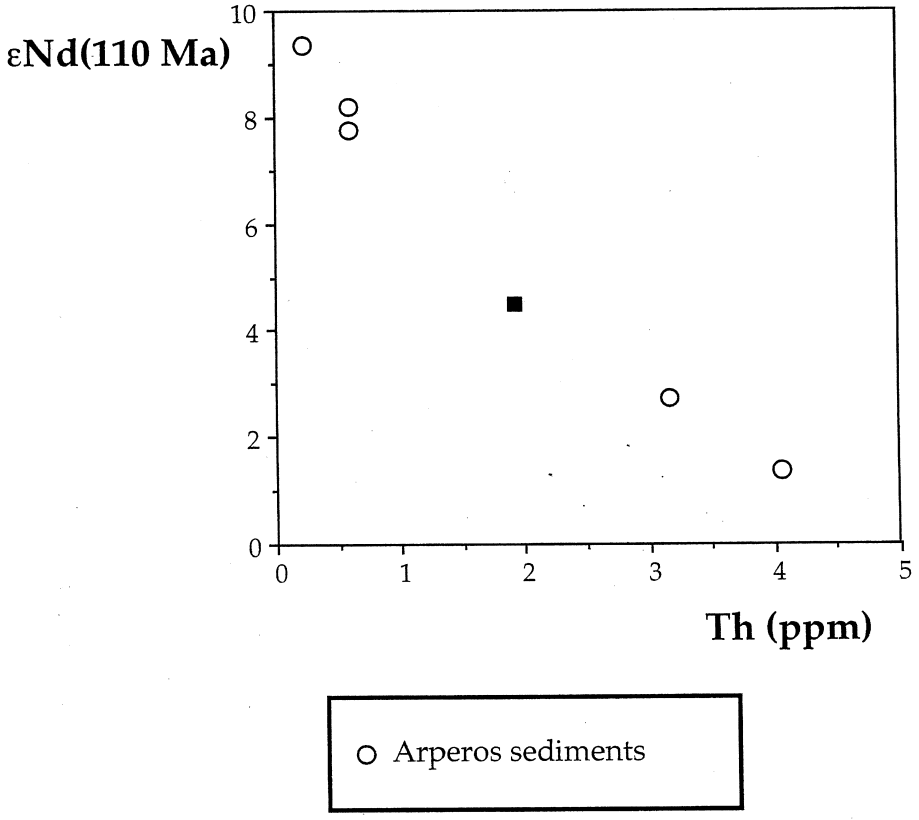

Fig. 8. Initial $\epsilon Nd_{(T=110\ Ma)}$ versus Th (ppm) plot for sediments from the Arperos basin.

that an Early Cretaceous marine basin floored by oceanic crust, and thickened by plume magmas, divided the Guerrero arc from nuclear Mexico. This basin was filled first by sediments derived from the ocean floor and/or the arc, and then by more evolved sources that could include nuclear Mexico. The oceanic affinity of the igneous floor of the Arperos basin and the primitive source of most of its sediments outline the juvenile characteristic and intra-oceanic environment of the Guerrero arc.

Acknowledgements

This work was funded by the DBT-INSU program (Contribution CNRS-INSU-DBT, Thème Dynamique Globale), URA-CNRS 69, and US NSF grants EAR-911726X and EAR-9316255. The W.M. Keck Foundation funded the ICPMS used for Th and REE analyses of the sediments. The authors wish to thank Drs James Gleason and Jonathan Patchett for their assistance with sediment analyses. C.F. would also like to thank Dr Louis Briqueu (Montpellier) for his help with the neodymium isotopic analysis of the volcanic rocks.

References

Almazan-Vazquez, E., 1988. Marco paleosedimentario y geodinamico de la Formacion Alisitos en la Peninsula de Baja California. Universidad Nacional Autonoma de Mexico, Instituto de Geologia, Revista, Vol. 7 (1), pp. 41–51.

Birck, J.L., Allègre, C.J., 1978. Chronology and chemical history of the parent body of basaltic achondrites studies by the $^{87}Sr/^{86}Sr$ method. Earth and Planetary Sciences Letters 94, 1–21.

Bonneau, M., 1972. Données nouvelles sur les séries crétacées de la côte pacifique du Mexique. Société Géologique de France, Sér. 7, Bulletin 24, 55–65.

Brouxel, M., Lapierre, H., Richard, A., Albarede, F., 1987. The deep layers of a Paleozoic arc: geochemistry of the Copley-Balaklala Series, northern California. Earth and Planetary Sciences Letters 85 (4), 386–400.

Campa, M.F., 1985. The Mexican Thrust Belt. In: Howell, D.G. (Ed.), Tectonostratigraphic Terranes of the Circum-Pacific Region. Circum Pacific Council Energy Mineral Resources, Earth Sciences Series, Vol. 1, pp. 299–313.

Campa, M.F., Coney, P.J., 1983. Tectono-stratigraphic terranes and mineral resources distribution in Mexico. Canadian Journal of Earth Sciences 20, 1040–1051.

Campa, M.F., Ramirez, J., 1979. La Evolucion Geologica y la Metalogenesis del Noroccidente de Guerrero. Universidad de Guerrero, Serie Tectonico Cientifica, 102 p.

Centeno-Garcia, E., Ruiz, J., Coney, P.J., Patchett, P.J., Ortega-Gutierrez, F., 1993. Guerrero terrane of Mexico: its role in the Southern Cordillera from new geochemical data. Geology 21, 419–422.

Coney, P.J., 1989. The North American Cordillera. In: Ben-Avraham, Z. (Ed.). Evolution of the Pacific Ocean Margins, Oxford University Press, Oxford, pp. 43–52.

Davila-Alcocer, A.V., Martinez-Reyes, J., 1987. Una edad cretacica para las rocas basales de la Sierra de Guanajuato. In: Resumenes del Simposio sobre la Geologia de la Sierra de Guanajuato. Instituto de Geologia, Universidad Nacional Autonoma de Mexico, pp. 19–20.

Evensen, N.M., Hamilton, P.J., O'Nions, R.K., 1978. Rare earth abundances in chondritic meteorites. Geochimica et Cosmochimica Acta 42, 1999–2212.

Freydier, C., Lapierre, H., Briqueu, L., Tardy, M., Coulon, C., Martinez-Reyes, J., 1996a. Volcaniclastic sequences with continental affinities within the Late Jurassic–Early Cretaceous Guerrero intra-oceanic arc (western Mexico). Journal of Geology 105, 483–502.

Freydier, C., Martinez, R.J., Lapierre, H., Tardy, M., Coulon, C., 1996b. The Early Cretaceous Arperos Basin (western Mexico): geochemical evidence for an aseismic ridge formed near a spreading center. Tectonophysics 259, 343–367.

Freydier, C., Martinez, R.J., Lapierre, H., Tardy, M., Coulon, C., 1998. The Early Cretaceous Arperos Basin (western Mexico): geochemical evidence for an aseismic ridge formed near a spreading center–Reply. Tectonophysics 292, 327–331.

Hollocher, K., Ruiz, J., 1995. Major and trace element determinations on NIST glass standard reference material-611, material-12, material-614, and material-1834 by inductively-coupled plasma-mass spectrometry. Geostandard Newsletter 19 (1), 27–34.

Lapierre, H., Brouxel, M., Albarède, F., Coulon, C., Lécuyer, C., Martin, P., Rouer, O., 1987. Paleozoic and Lower Mesozoic magmas from the eastern Klamath Mountains (N. California). Tectonophysics 140, 155–177.

Lapierre, H., Ortiz, H.E., Abouchami, N.V., Monod, O., Coulon, C., Zimmermann, J.-L., 1992a. A crustal section of an intra-oceanic island arc: The Late Jurassic–Early Cretaceous Guanajuato magmatic sequence (central Mexico). Earth and Planetary Sciences Letters 108, 61–77.

Lapierre, H., Tardy, M., Coulon, C., Ortiz-Hernandez, E., Bourdier, J.L., Martinez-Reyes, J., Freydier, C., 1992b. Caractérisation, genèse et évolution géodynamique du "Guerrero terrane" (Mexique occidental). Canadian Journal of Earth Sciences 29, 2478–2489.

Lapierre, H., Bosch, D., Dupuis, V., Polvé, M., Maury, R.C., Hernandez, J., Monié, P., Yeghicheyan, D., Jaillard, E., Tardy, M., Mercier de Lépinay, B., Mamberti, M., Desmet, A., Keller, F., Sénebier, F., 2000. Multiple plume events in the genesis of the peri-Caribbean Cretaceous oceanic plateau province. Journal of Geophysical Research-Solid Earth 105 (B4), 8403–8421.

Nakamura, N., 1974. Determination of REE, Ba, Fe, Mg, Na and K in carbonaceous and ordinary chondrites. Geochimica et Cosmochimica Acta 38, 757–775.

Ortiz-Hernandez, E.L., Yta, M., Talavera, O., Lapierre, H., Monod, O., Tardy, M., 1991. Origine intra-océanique des formations volcano-plutoniques d'arc du Jurassique supérieur-Crétacé inférieur du Mexique centro-méridional. Comptes Rendus de l'Académie des Sciences (Paris), Série II 305, 1093–1098.

Ortiz-Hernandez, E.L., 1992. L'Arc Intra-Océanique Allocthone Jurassique Supérieur-Crétacé Inférieur du Domaine Cordillérain Mexicain ("Guerrero Terrane"): Pétrographie, Géochimie et Minéralisations Associées des Segments de Guanajuato et de Palmar Chico-Arcelia–Conséquences Paléogéographiques. Thèse, Université Joseph Fourier-Grenoble, 109 p.

Patchett, P.J., Ruiz, J., 1987. Nd isotopic ages of crust formation and metamorphism in the Precambrian of eastern and southern Mexico. Contributions to Mineralogy and Petrology 96, 523–528.

Richard, P., Shimizu, P., Allègre, J.C., 1976. $^{143}Nd/^{144}Nd$, a natural tracer: an implication to oceanic basalt. Earth and Planetary Sciences Letters 31, 269–278.

Salinas-Prieto, J.C., 1994. Étude Structurale du SW Mexicain (Guerrero): Analyse Microtectonique des Déformations Ductiles du Tertiaire Inférieur. Thèse, Université d'Orléans, 211 p.

Samson, S.D., Patchett, P.J., Gehrels, G.E., Anderson, R.G., 1990. Nd–Sr isotopic characterisation of the Wrangellia terrane and implications for crustal growth of the Canadian Cordillera. Journal of Geology 98, 749–762.

Sun, S.S., McDonough, W.F., 1989. Chemical and isotopic systematics of oceanic basalts: Implications for mantle composition and processes. In: Saunders, A.D., Worry, M.J. (Eds.). Magmatism in the Ocean Basins, Geological Society of London, pp. 313–345 (Special Publication 42).

Tardy, M., Carfantan, J.C., Rangin, C., 1986. Essai de synthèse sur la structure du Mexique. Bulletin de la Société Géologique de France 8(II) (6), 1025–1031.

Tardy, M., Lapierre, H., Freydier, C., Coulon, C., Gill, J., Mercier de Lépinay, B., Beck, C., Martinez-Reyes, J., Talavera-Mendoza, O., Ortiz-Hernandez, E., Stein, G., Bourdier, J.-L., Yta, M., 1994. The Guerrero suspect terrane (western Mexico) and coeval arc terranes (the Greater Antilles and the Western Cordillera of Colombia): A late Mesozoic intra-oceanic arc accreted to cratonal America during the Cretaceous. Tectonophysics 230, 49–73.

Vicenzi, E., McBirney, A.R., Duncan, R.A., 1990. The geology and geochemistry of Isla Marchena, Galapagos Archipelago: an ocean island adjacent to a mid-ocean ridge. Journal of Volcanic and Geothermal Research 40, 291–315.